GE-International Journal of Engineering Research
Vol. 4, Issue 8, August 2016 IF- 4.721 ISSN: (2321-1717)
© Associated Asia Research Foundation (AARF) Publication
Website: www.aarf.asia Email : editor@aarf.asia , editoraarf@gmail.com

DIELECTRIC AND IMPEDANCE SPECTROSCOPIC STUDIES OF IRON DOPED YTTRIUM COPPER TITANATE CERAMICS

S. Sharma[1] and K.D. Mandal[1]

[1] Department of Chemistry, Indian Institute of Technology (Banaras Hindu University), Varanasi, 221005, (U.P.), India.

ABSTRACT

The electrical properties of iron doped $Y_{2/3}Cu_3Ti_4O_{12}$ pellets were investigated by impedance and dielectric spectroscopy in the frequency range 2Hz-5MHz from 308-500 K. Powders of Nano-sized $Y_{2/3}Cu_3Ti_{4-x}Fe_xO_{12}$ (x = 0.00, 0.05, 0.10, 0.15 and 0.20) ceramics were synthesized by semi-wet route which employs solid TiO_2. The impacts of doping of Ti^{4+} site by Fe^{3+} on $Y_{2/3}Cu_3Ti_4O_{12}$ ceramic were reflected as a decrease in the grain size with a significant lowering of dielectric loss in comparison to the undoped YCTO ceramic. The loss tangent of $Y_{2/3}Cu_3Ti_{4-x}Fe_xO_{12}$ (x = 0.20) ceramic drops to 0.05 at a frequency of 1 kHz, a reduction by 55% in comparison to pure YCTO ceramic. The origin of high dielectric constant in all samples along with their rationalization with the help of impedance spectroscopic analysis has been discussed. All compositions were found to be electrically heterogeneous with semiconducting grains and insulating grain boundaries, supporting IBLC mechanism.

KEYWORDS - Nano-ceramic; Miniaturization; Semi-wet route; Perovskite oxides; Dielectric dispersion.

INTRODUCTION

With recent advancements in miniaturization and integration in device manufacturing processes, it is intriguing to develop some new type of capacitors with high dielectric

constant and stable temperature characteristics. Considerable research efforts have been distinctly manifested to develop new materials exhibiting high dielectric constant for applications in microelectronics industries leading to a fast growing field of science, both in the field of novel materials and their applications in future packing technologies [1-3]. Traditional $BaTiO_3$ (BT) and $PbZr_xTi_{1-x}O_3$ (PZT) based ferroelectric materials also exhibit high dielectric constant. But the dielectric properties of these materials are strongly temperature-dependent due to phase transition at Curie temperature, which restricts their application in high temperature range. Further Lead containing ceramics, being poisonous and eco-unfriendly, it is desirable to fabricate some non-ferroelectric materials with high dielectric constant to substitute these traditional ferroelectrics. Materials with the general formula $ACu_3Ti_4O_{12}$ (A = Ca, Ba, Sr) crystallize as body centered cubic perovskite-related structures in space-group *Im*3. One of the most recognized ceramics, $CaCu_3Ti_4O_{12}$ (CCTO) has been studied since the last one decade owing to its giant dielectric constant ($\varepsilon_r \sim 10^4$ for bulk and 10^5) for single crystal and moderately low dielectric loss (~ 0.10) despite its centrosymmetric nature with BCC structure (lattice parameter, a =7.391Å). CCTO has got advantage over $BaTiO_3$ because its dielectric constant remains nearly temperature independent (100 – 600 K) and frequency independent (10^2-10^6Hz) without any structural phase transition [4]. Such type of temperature independent behavior of CCTO is technically appealing alternative for the currently used ferroelectric materials and for the development of future microelectronic devices, with the same time suggesting itself a potential for technological applications, especially in memory devices specifically in dynamic random access memory (DRAMs), capacitive components or microwave devices, due to the possibility to reduce the dimensions needed in microelectronic equipments [5].

The correlation between the crystal structure and intrinsic dielectric properties of the unusual cubic perovskite based compounds of $ACu_3Ti_4O_{12}$ family has been a controversial issue for several years, exclusively for $CaCu_3Ti_4O_{12}$ (CCTO) family, the most studied member. Different mechanisms have been proposed to interpret the origin of giant dielectric response of CCTO. The giant dielectric response in CCTO may be supposed either due to disorder caused at Ca/Cu-site in CCTO crystal or due to an extrinsic mechanism caused by internal barrier layer capacitance (IBLC) model [6]. The IBLC mechanism has been widely accepted but is still controversial. Some researchers correlate this phenomenon to origin of local dipole moments associated with the displacement of some ions or due to relaxor behavior like dynamical slowing down of dipolar fluctuations in nano-size domains or off-centric displacement of Ti^{4+} ions within TiO_6 octahedra within CCTO molecule [7]. Various

research papers revealed that the dielectric response of CCTO is significantly influenced by factors like processing routes and conditions applied during its fabrication like sintering temperature and its duration, cooling rate and partial pressure of the sintering atmosphere. Apart from this, doping schemes as well as nature of dopants and their stoichiometric variations affecting the microstructure of the material and the measuring frequency and temperature range are quite important [8]. Various papers describing substitution effect of dopants on dielectric properties of CCTO has been reported earlier are scattered in literature.

The structural isomorphs of $ACu_3Ti_4O_{12}$ materials with a general formula $A_{2/3}Cu_3Ti_4O_{12}$ (A = $Y_{2/3}$, $Bi_{2/3}$, $La_{2/3}$) also show similar dielectric properties and are also reported in literature. Structural isomorphs of $A_{2/3}Cu_3Ti_4O_{12}$ (ACTO) where A is a rare earth metals have gained tremendous research attraction due to its various possible applications in microelectronics, high energy density storage applications and high performance dielectric devices. Such compounds could also be a promising candidate to replace relaxors as dielectrics. Apart from this, a wide variety of doping or partial substitution may be carried out at the A, Cu or Ti-site of ACTO, which may be suitable for different industrial applications such as dynamic and versatile memory components, capacitors, transducers and sensors etc. The choice of substituent to modify the physical properties of the material is based on many factors including charge neutrality, tolerance factor, the ionic radius and solubility. As we know partial isovalent substitution of metal cations in different interstices can improve properties associated with ferroelectricity and dielectric response in these materials due to the partial modification of mixed-valent structure. Further, structural flexibility and chemical versatility of the materials make them more suitable for device applications [9] and it is quite inspiring to investigate systematically new $ACu_3Ti_4O_{12}$ like materials. A detail literature survey shows that not much work has been reported on $Y_{2/3}Cu_3Ti_4O_{12}$ (YCTO) compound which is isostructural to CCTO which may offer a large database to search for high dielectric constant materials [10-13]. Being non-ferroelectric, lead-free and eco-friendly too, YCTO material exhibits a high dielectric constant with good thermal stability. However, the dielectric loss (tan δ) of this material is high which is the main obstacle limiting its technical use. But due to advantage of flexible structure, properties can be modified by changing the chemical compositions through different possible substitutions at Y^{3+}, Cu^{2+} or Ti^{4+} sites. To our best knowledge, no work on the effects of substituting impurity in YCTO at a lower processing temperature has been reported. Presently, we have worked out to control the dielectric loss factor by doping of Fe^{3+}at Ti^{4+} site in continuation to a detail research work on YCTO system.

In the present communication, we are reporting the cationic substitution of Ti^{4+} site by doping the heterovalent Fe^{3+} ions in YCTO. The different proportion of Fe^{3+} was introduced into YCTO system to synthesize the single phase iron doped $Y_{2/3}Cu_3Ti_{4-x}Fe_xO_{12}$ (x = 0.00, 0.05, 0.10, 0.15 and 0.20) samples by the semi-wet route at a relatively lower sintering temperature 1000 ^oC. The effects of Fe^{3+}-doping on the structural and dielectric properties of YCTO ceramics were studied. Also, the rationalization of dielectric behavior with the help of impedance spectroscopic study along with mechanism of electrical conductivity affecting the dielectric loss of Fe^{3+}-doped YCTO ceramics has been illustrated in the paper.

EXPERIMENTAL

MATERIAL SYNTHESIS

Different samples of $Y_{2/3}Cu_3Ti_{4-x}Fe_xO_{12}$ ceramics (x = 0.00, 0.50, 0.10, 0.15 and 0.20) were synthesized by semi-wet route using analytical grade chemicals $Y(NO_3)_3.6H_2O$ [99%, HiMedia, India], $Cu(NO_3)_{2.}3H_2O$ [99.5%, Merk, India], $Fe(NO_3)_{3.}9H_2O$ [99.8%, Merk, India], TiO_2 [99.5%, Merk, India], and glycine [99.5%, Merk, India], as starting materials. Standard solutions of these metal nitrates were prepared using double distilled water. Solutions of metal nitrates in stoichiometric amount of these metallic ions were mixed in a beaker and a calculated amount of TiO_2 and glycine, equivalent to metal ions, were added to the solution. The solution was heated on a hot plate with constant stirring using a magnetic stirrer at 70-80 ^oC to evaporate water till blue gel was obtained. After combustion of blue gel, dry powder was obtained. Thermal studies were carried out for the dry powder using TG/DTA (Pyris Diamond TG/DTA, Perkin Elmer Instrument, USA) with heating rate 10 ^oC per minute from ambient to 1000 ^oC. The dry powder was calcined in air at 500 ^oC and 800 ^oC for 5h and 8h respectively in a muffle furnace. The calcined powder was ground into fine powder and then pressed into cylindrical pellets of dimension 12 mm in diameter and 1.6 mm in thickness using a hydraulic press by applying uniaxial pressure of 4 ton. Poly vinyl alcohol (PVA) was used as a binder to reduce the brittleness of pellets. The pressed pellets were again heated to 500 °C to remove the binder by the burn-out process and then sintered in air at 1000 ^oC for 12h in air for different physiochemical characterizations.

MATERIAL CHARACTERIZATION

Density and porosity of all the five compositions of $Y_{2/3}Cu_3Ti_{4-x}Fe_xO_{12}$ (x = 0.00, 0.50, 0.10, 0.15 and 0.20) sintered at 1000 ^oC were measured with the help of Archimedes Principle. The

crystalline phase structure of all compositional variant were identified using an X-ray diffractometer (D/max-2550/PC, Rigaku, Tokyo, Japan) employing Cu-K_α radiation (λ=1.5414 Å). The morphology of the fractured surfaces of different compositional variant YCTFO ceramic were characterized by scanning electron microscopy (SEM, Model JEOL JSM5410) and transmission electron microscopy (TEM, FEI Tecnai-20G^2) with an accelerating voltage of 200 kV. For TEM analysis, powder form of sintered ceramic of each composition was dispersed in acetone differently and 1-2 drops of each were mounted on a carbon coated copper grid. The solvent was subsequently allowed to escape in air at room temperature. For dielectric measurements, both the flat and parallel surfaces of one pellet of each compositional variant was polished and coated by air drying conducting silver paint. To form electrodes, required for further electrical characterizations, those pellets were dried at 200 ^oC for 30 minutes to remove moisture, if any, and then cooled at room temperature, before taking electrical measurements. Dielectric measurement data were taken by LCR meter (PSM1735-NumetriQ, Newton 4th Ltd, U.K.) in a wide range of frequency 2Hz – 5MHz at different temperature 35-227 ^oC. The value of dielectric constant was evaluated using the standard relation, $\varepsilon_r = Cd/\varepsilon_0 A$, where C is capacitance, d is the thickness of the pellet, A is the effective cross sectional area of the pellet and $\varepsilon_0 = 8.854\times10^{-12}$ F/m.

RESULTS AND DISCUSSION

TGA/DTA Studies

To ascertain the ideal temperature required for the thermal decomposition of precursor dry powder of $Y_{2/3}Cu_3Ti_{4-x}Fe_xO_{12}$ ceramic, TG/DTA was carried out. Fig. 1 shows simultaneous TG/DTA/DTG plots of precursor powder of $Y_{2/3}Cu_3Ti_{4-x}Fe_xO_{12}$ ceramic (x = 0.20) ceramic. Two major stages of weight loss in the temperature range from 100 ^oC to 1000 ^oC was observed in TGA plot, the first major weight loss at 250 ^oC is due to an exothermic reaction which may be attributed to dehydration and combustion of the gel while the second weight loss at 800 ^oC is due to the formation of an intermediate compound. Further, an additional but very small weight loss at 950 ^oC was also observed which is due to an exothermic addition reaction of the intermediate compound to give the final product $Y_{2/3}Cu_3Ti_{4-x}Fe_xO_{12}$ (x = 0.20). The corresponding DTA and DTG plot also show two strong exothermic peaks near 250 ^oC and 850 ^oC besides a small peak at 950 ^oC. It was also observed that DTG peaks are more intense than DTA peaks.

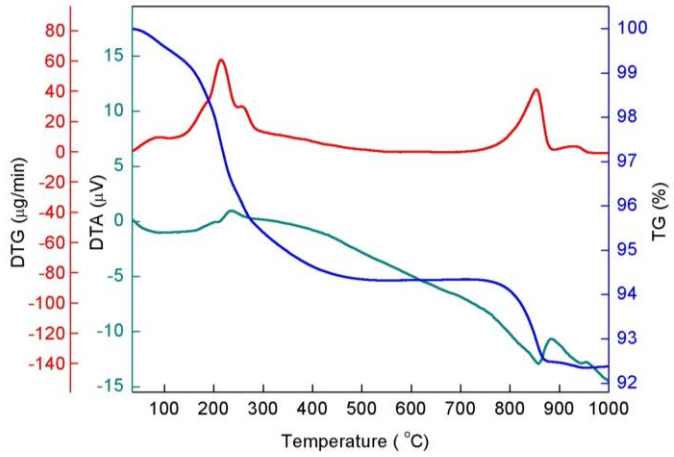

Figure 1 : DTA/TGA Curve for Precursor Powder of $Y_{2/3}Cu_3Ti_{4-x}Fe_xO_{12}$ Ceramic (x = 0.20).

Crystal Structure

XRD pattern of all the five compositions of $Y_{2/3}Cu_3Ti_{4-x}Fe_xO_{12}$ (x = 0.00, 0.50, 0.10, 0.15 and 0.20) ceramic sintered at 1000 ^oC for 12 h is illustrated in Fig. 2. It clear from the Fig 2 that all the compositional variants show distinct diffraction peaks corresponding to (211), (220), (013), (222), (321), (400), (422), (440) orientations which were found to have a good matching with $CaCu_3Ti_4O_{12}$ (JCPDS card no. 75-2188), demonstrating thus a polycrystalline characteristic of YCTFO ceramics. In addition to a dominant pure $CaCu_3Ti_4O_{12}$ (CCTO) phase, Fig 2 indicates the presence of small amounts of CuO as a minor, secondary phase of CuO (JCPDS 80-1917). The curves of sample with x = 0.05-0.20 were almost identical with that of x = 0.00 and with the same time not a single Fe-related phase was detected in the XRD patterns with Fe^{3+} up to x = 0.20, which indicated that Fe^{3+} hadn't influenced the crystalline nature. At the same time, no significant secondary phase could be detected in the XRD data, for the samples with x = 0.05-0.20, probably because their quantities may be lower than the detection limits of the technique. It is also clear from the Table 1 that the lattice constant increases monotonically with increasing of x values. It indicates that the Fe^{3+} may have taken the place of Ti^{4+} as expected. The increase of the lattice constant is with doping concentration is may be either due to the difference in ionic radii of the dopent Fe^{3+} (0.785Å) to that of parent Ti^{4+} (0.745Å) ion and thus causing a decrease in defect density due to doping.

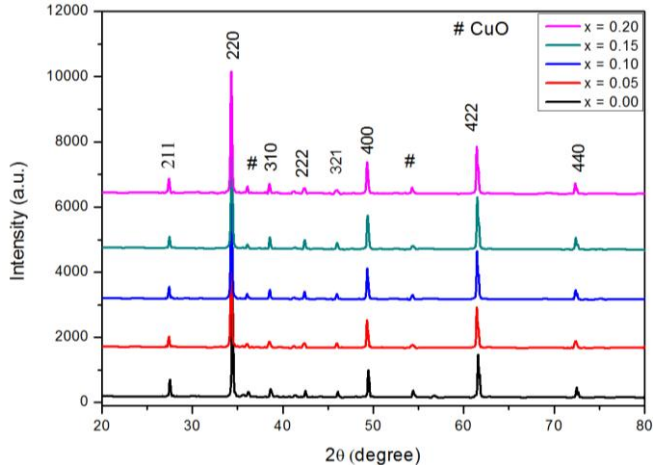

Figure 2 : XRD Patterns of $Y_{2/3}Cu_3Ti_{4-x}Fe_xO_{12}$ Ceramic (x = 0.00, 0.05, 0.10, 0.15 and 0.20) Sintered at 1000 ^oC for 12 h.

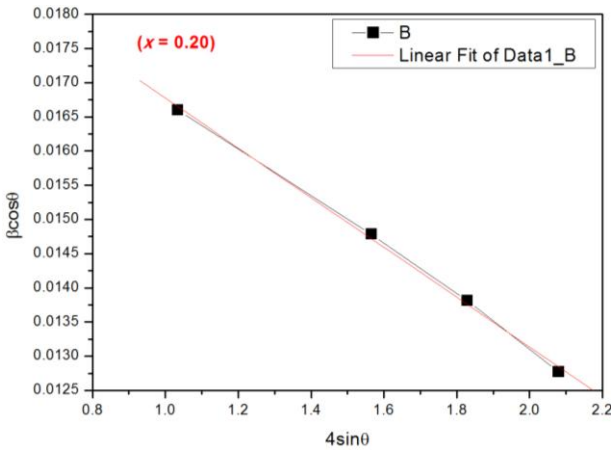

Figure 3: Williamson-Hall Plot for Sintered $Y_{2/3}Cu_3Ti_{4-x}Fe_xO_{12}$ (x = 0.20) Ceramic.

XRD data were indexed on the basis of a cubic unit cell similar to CCTO. The lattice parameter and unit cell volume of different compositional YCTFO ceramic were determined by least squares refinement method using 'Cel' software and is listed in Table 1. The presence of split peaks in XRD pattern for the reflections 400, 422 and 440 may be due to the presence of Cu-Kα_2 along with Cu-Kα_1 in the X-ray radiations used for diffraction. It is supported by the fact that in all these reflections, the intensity of peaks due to Cu-Kα_2 is close to 50% of intensity of peak due to Cu Kα_1 as expected [14].

The crystallite size (D) of the different YCTFO ceramic were estimated using the Debye-Scherrer's formula, as shown in equation (1)

$$D = \frac{k\lambda}{\beta \cos\theta} \quad (1)$$

where k is the crystal shape coefficient (k = 0.89), λ is the wave length of X-ray radiation, θ is the diffraction angle and β is the corrected full width at half maximum (FWHM) obtained after correcting the peak broadening due to instrument and lattice strain [15]. For correction in peak broadening a few main peaks with greater intensity within the XRD pattern were selected for $Y_{2/3}Cu_3Ti_{4-x}Fe_xO_{12}$ (x = 0.20) sample. The silicon wafer was taken as a reference material to determine the peak broadening due to instrument. Knowing the slope and intercept of the straight line obtained by Williamson-Hall Plot (shown in Fig. 3), lattice strain and the actual crystallite size (D) for the sample x = 0. 20 were determined to be 0.36% and 6.819 nm respectively [16]. The calculated value of crystallite size, after correction in the instrumental broadening for different $Y_{2/3}Cu_3Ti_{4-x}Fe_xO_{12}$ (x = 0. 00, 0.10, 0.15 and 0.20) ceramics are also shown in Table 1. These are also in the nano-particle range.

Table 1: Crystal Structure, Lattice Parameter and Unit Cell Volume of $Y_{2/3}Cu_3Ti_{4-x}Fe_xO_{12}$ (x = 0.00, 0.05, 0.10, 0.15 and 0.20) Ceramic

System	Composition	Crystal Structure	Lattice Parameter (Å)	Unit Cell Volume $(Å)^3$	Crystallite Size (nm)
$Y_{2/3}Cu_3Ti_{4-x}Fe_xO_{12}$	x = 0.00	Cubic	7.4983	421.5833	68 ± 6
	x = 0.05	Cubic	7.5149	424.3867	64 ± 9
	x = 0.10	Cubic	7.5339	427.6257	62 ± 8
	x = 0.15	Cubic	7.5173	424.7931	60 ± 7
	x = 0.20	Cubic	7.5200	425.2557	58 ± 6

Microstructural analysis

The scanning electron micrograph (SEM) of the fractured surfaces of $Y_{2/3}Cu_3Ti_{4-x}Fe_xO_{12}$ (x = 0.00, 0.50, 0.10, 0.15 and 0.20) ceramic sintered at 1000 ^oC for 12h are shown in Fig. 4(a-e). The SEM micrograph exhibits non-uniform grain size distribution consisting of bimodal nature with frequent segregation. The microstructure is dominated by small smooth surfaced grains with some pores. The grains have geometrical patterns like spherical, cylindrical and cubical in Fig. 4(a-d) while some are hexagonal in Fig. 4(e). It is clear from the picture that the grains are still in growing condition which is suggested by the variation in sizes of spherical, cylindrical and cubical structures as well. The bimodal grain size distribution contains regions of fine grains about ~0.5-1 μm and regions of extremely large grains about ~1.5-3.5 μm for all compositions with high degree of segregation. The composition of smaller and larger grains coincides with the stoichiometry of the chemical formula of $Y_{2/3}Cu_3Ti_{4-x}Fe_xO_{12}$ (x = 0.00, 0.50, 0.10, 0.15 and 0.20) which is also supported by EDX results. The variation in grain size thereby leading to abnormal grain growth may be due to the presence of CuO rich phase at the grain boundary of the ceramic.

Fang *et al* also reported the presence of CuO along the grain boundary which transforms into the liquid phase during sintering it may induce discontinuous grain growth [17] which is in accordance with the SEM micrograph of Fig. 4. The CuO phase may contribute significant effects to promote the grain growth and densification of YCTFO samples. Fig 4(a) shows a discontinuous grain growth for the pure sample; however, a continuous grain growth can be seen clearly for all the samples with doping of iron with a decrease in the average grain size from 0.61-52 μm for smaller grains and 3.14-2.30 μm for larger grains. The doping of iron has effectively prevented the growth of large grains and average grain sizes are approximately 0.5~3.5 μm which is independent of Fe^{3+} concentration (shown in Fig. 4b~d). It indicates that the adding of Fe^{3+} with variable concentration can reduce the grain size of YCTFO ceramic and improve the density of the ceramic. The bulk density of the samples was measured and found to be 1.19. 1.67, 1.33, 1.29, and 1.28 for x = 0.00, 0.05, 0.10, 0.15 and 0.20, respectively, considering the theoretical density of 5.995 g/cc for YCTO [13]. Such variation in density of these samples may be due to the presence of some pores in YCTFO samples.

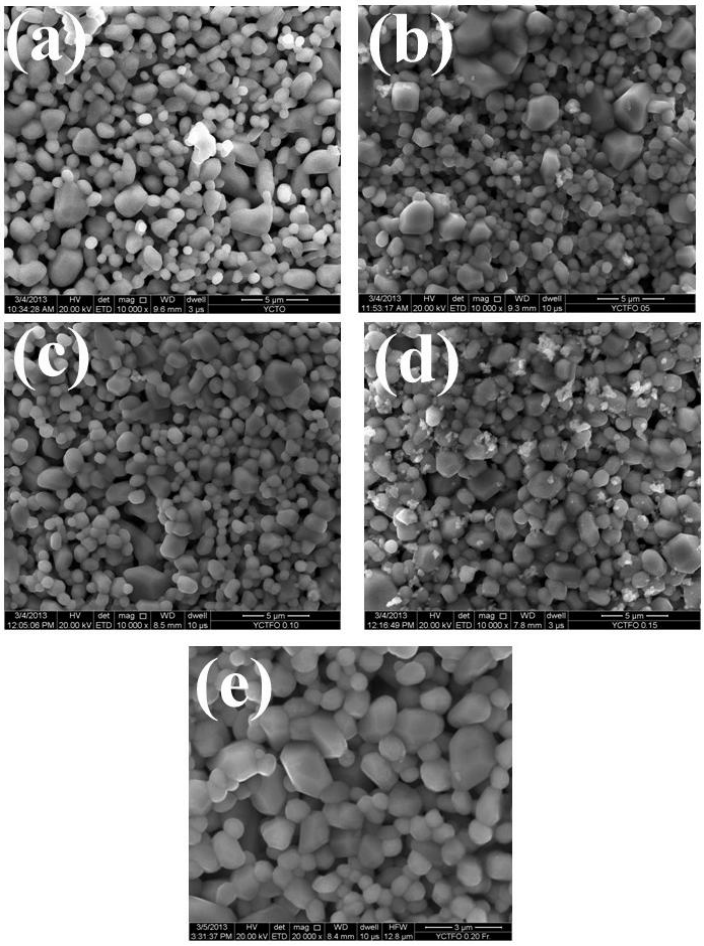

Figure 4: Scanning Electron Micrographs of $Y_{2/3}Cu_3Ti_{4-x}Fe_xO_{12}$ (a) x = 0.00, (b) x = 0.05, (c) x = 0.10, (d) x =

0.15 and (e) x = 0.20 Sintered at 1000 $^{\circ}$C for 12h.

It is also established that increase in sintering temperature significantly promote the grain growth and microstructural densification. It is quite obvious that with decrease in average size to those of smaller and larger grain, porosity decreases leading to more compactness of YCTFO ceramics. Further, it is reported in literature that below 1µm, the dielectric constant decreases significantly with grain size. As the grain size approaches to 0.5-1.5 µm, the various types of stress operating in the grain suppress the domain and the dielectric constant falls to approximately 1000 [1]. Such type of relation between the grain size and dielectric constant value are reflected as well for different YCTFO ceramic samples. Besides grain size in the range of 0.5-1.5 µm, all iron doped YCTO ceramic exhibits a low dielectric constant value (ε_r ~ 380, 351, 881, 1275) than the pure YCTO ceramic (ε_r ~ 2198) with grain size in the range of 1-3µm which may be due to porosity, compactness of grain and the structural quality of the material. It is also clear from the Fig. 4 that for different

YCTFO ceramic samples exhibits high degree of porosity. The calculated values of porosity are listed in the Table 2.

The high porosity may be attributed to the formation of oxygen vacancies during sintering. It may be also due to lower sintering temperature. Increase in sintering temperature may lead to decrease in porosity owing to the grain growth phenomena. Moreover, the porosity also depends upon processing route, samples prepared by Pechini method and co-precipitation method exhibit a lower extent of porosity than those prepared by other processes at the same sintering temperature [18]. It was also observed that doping of Fe in YCTO ceramic resulted in decrease in density and increase in porosity. Density of different samples of YCTFO samples are in accordance with the reported value of undoped YCTO ceramic [13].

Table 2: Pellet Dimension, Density and Porosity Characteristic for Different $Y_{2/3}Cu_3Ti_{4-x}Fe_xO_{12}$ Ceramic Sintered at 1000 $^{\circ}$C for 12 h.

System	Composition	Pellet Dimension (mm)		Density		Porosity	
		Thickness	Diameter	Theoretical	Bulk	Bulk	Apparent
$Y_{2/3}Cu_{3-x}Ti_{4-x}Fe_xO_{12}$	x = 0.00	3.5	12.5	5.995	1.195	80.06	22.02
	x = 0.05	2.0	9.0	5.950	1.167	80.38	11.19
	x = 0.10	3.0	9.0	5.895	1.337	77.32	30.38
	x = 0.15	2.0	9.0	5.925	1.291	78.21	18.67
	x = 0.20	2.0	10.5	5.909	1.287	78.21	14.16

Fig. 5 shows EDX spectra of grain of different compositions of $Y_{2/3}Cu_3Ti_{4-x}Fe_xO_{12}$ which indicates the presence of Y, Cu, Ti, Fe and O elements. Quantitative data for atomic and weight percentage of the elements present in the grain of YCTFO obtained from EDX

data which is shown in Table 3. The atomic percentage of Y, Cu, Ti, Fe and O in different compositions of $Y_{2/3}Cu_3Ti_{4-x}Fe_xO_{12}$ ceramics was as per expected stoichiometry.

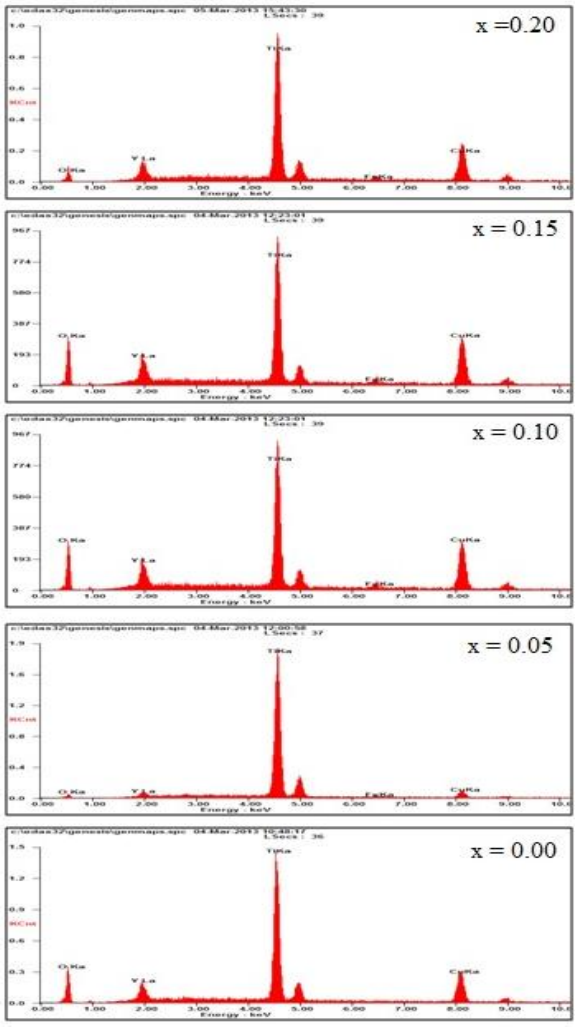

Figure 5: EDX spectra of grain surface of sintered $Y_{2/3}Cu_3Ti_{4-x}Fe_xO_{12}$ ceramic (x = 0.00, 0.05, 0.10, 0.15 and

0.20).

Table 3: Atomic Percentage and Weight Percentage of Elements for $Y_{2/3}Cu_3Ti_{4-x}Fe_xO_{12}$ Ceramic (x = 0.00, 0.05,

0.10, 0.15, 0.20) Sintered at 1000 $^{\circ}$C for 12 h.

System	Composition	Region	Wt%					At%					
			Y	Cu	Fe	Ti	O	Y	Fe	Cu	O	Ti	
$Y_{2/3}Cu_{3-x}Ti_{4-x}Fe_xO_{12}$	x =0.00	(Grain)	08.94	33.76	33.36	----	23.95	03.56	18.80	24.65	----	52.99	
	x = 0.05	(Grain)	08.40	32.94	37.91	1.68	19.06	03.60	19.74	30.14	01.14	45.37	
	x = 0.10	(Grain)	08.07	36.76	40.21	1.65	13.31	03.38	24.41	35.42	01.25	35.09	
	x = 0.15	(Grain)	08.28	36.67	29.95	1.99	36.67	03.36	20.80	22.53	01.28	20.80	
	x = 0.20	(Grain)	07.91	33.19	38.28	2.19	18.43	03.42	20.08	30.72	01.51	44.28	

The bright field TEM image of YCTFO ceramic sintered at 1000 ^{o}C for 12h is represented in Fig. 6(a-c). In the vicinity of composition with concentration of x = 0.00, 0.05 and 0.10 only, a distinguished TEM image are produced. The particles of different compositions of $Y_{2/3}Cu_3Ti_{4-x}Fe_xO_{12}$ are well dispersed with high extent of agglomeration. The average particles are in the range of 20 ± 7 nm. The lattice parameter calculated from the electron diffraction pattern is also in agreement with that obtained from the XRD data. However, the particle size obtained by TEM analysis is lesser than XRD results because a crystallite may consist of several particles. TEM diffraction pattern was indexed on the basis of body centred cubic perovskite structure. The corresponding selected area electron diffraction (SAED) pattern of TEM image for YCTFO ceramic is shown in Fig. 6(d). As the corresponding selected area electron diffraction (SAED) pattern of TEM image for different samples are more or less same, SAED picture for composition x = 0.20 only is reproduced here. The presence of a few clear rings in SAED pattern again confirms the formation of polycrystalline phase of thermodynamically stable YCTFO ceramic.

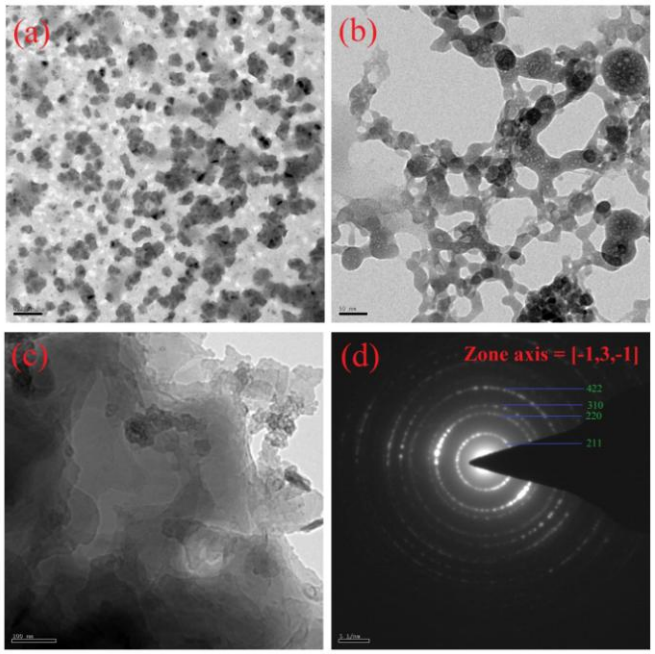

Figure 6: TEM Bright Field Image of Sintered $Y_{2/3}Cu_3Ti_{4-x}Fe_xO_{12}$ Ceramic where (a) x = 0.00 (b) x = 0.05

(c) x = 0.10 and (d) Corresponding SEAD Pattern for x = 0.20 Composition.

Dielectric spectroscopic studies

Fig. 7 exhibits the temperature dependence of dielectric (ε) and dielectric loss (tan δ) measured at a few frequencies for $Y_{2/3}Cu_3Ti_{4-x}Fe_xO_{12}$ (x = 0.00, 0.50, 0.10, 0.15 and 0.20) ceramic. It is clearly observed from Fig 7(a) that the YCTFO ceramic, with high concentration of Fe^{3+} (x = 0.20) exhibit step like increase in dielectric constant with increasing measuring temperature. Along with this dielectric peaks are also observable for almost all Fe^{3+} doped YCTFO compositions with x = 0.00, 0.10 and 0.20 near temperature 350-60 K while composition for compositions with x = 0.05 and 0.15, the dielectric peak appears to be suppressed one and exhibit almost temperature independent behaviour after temperature 425-500 K. Further, with increasing measuring frequency, increase in dielectric constant suppressed with amplitude which indicates that the existence of at least one Debye like relaxation in different YCTFO ceramics. In general, one Debye like relaxation is accompanied by the appearance of dielectric loss peak or hump in tan δ–T plot. As shown in Fig 7(b), only one dielectric loss peak is observed around 360 K for YCTFO ceramic for all concentration except x = 0.15. Although dielectric loss peak or hump is not observable for all concentration except x = 0.20. It is also noticeable that with increase in concentration of Fe, the hump in the low temperature range gets intensified in both ε-T and tanδ–T plots which

may be attributed to increase in the grain boundary resistance therefore it can be inferred that the observed low temperature dielectric relaxation supports the grain boundary effects. The appearance of high temperature dielectric loss hump for x = 0.20 might be attributed to higher conductivity at high temperature.

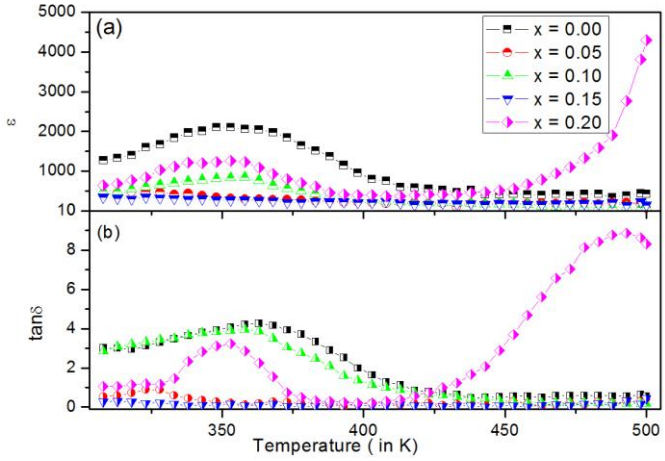

Figure 7: Plots of Dielectric Constant (ε′) and Loss Tangent (tan δ) with Temperature at few Selected

Frequencies for Sintered $Y_{2/3}Cu_3Ti_{4-x}Fe_xO_{12}$ Ceramic (x = 0.00, 0.05, 0.10, 0.15 and 0.20).

Fig. 8 illustrates the variation of real and imaginary part of dielectric constant (ε) with frequency for Fe^{3+} doped YCTFO ceramic sintered at 950^o C for 9 h within the frequency range 2Hz to 5MHz at different concentration. The values of dielectric constant (ε′) of YCTFO ceramic with different compositions are 100837, 32948, 43065, 29958 and 32376 respectively. All compositions exhibit a constant dielectric constant value 10^4-10^3 at the frequency 2 Hz to 5 MHz with a continuous decrease in the value of dielectric constant with frequency, however, this decrease is rapid in lower frequency range (2 Hz-100 Hz) and very slow in higher frequency range (1 kHz to 5 MHz). A large value of dielectric constant under frequency 2-100Hz may be associated to electrode contact while the drastic decrease in the value of dielectric constant at high frequency greater that f = 100 Hz thus suggests the presence of conductive grains. Furthermore, the rapid decrease in dielectric constant with frequency may be due to the contribution of space charge accumulation at the interface which leads to polarization of the ionic medium and hence the value of ε′ increases. In high frequency regions, the periodic reversal of the field takes place so rapidly that there is no charge accumulation at the interface, resulting into a constant ε′ value [19].

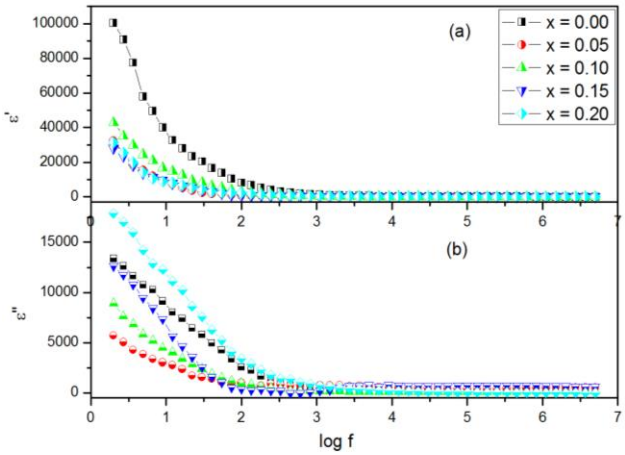

Figure 8: Plots of (a) Real Dielectric Constant (ε′) and (b) Imaginary Dielectric Constant (ε″) with Frequency at

Different Temperature for $Y_{2/3}Cu_3Ti_{4-x}Fe_xO_{12}$ Ceramic (x = 0.00, 0.05, 0.10, 0.15 and 0.20).

The frequency dependence of the imaginary part of dielectric constant (ε″) at room temperature for all compositions is shown in Fig 8(b). All the curves show an appreciable decrease in the loss magnitude. At high frequencies, the losses are much lower than the one occurring at low frequencies. Such kind of dependence of the dielectric loss with frequency is associated with losses due to the conduction mechanism.

The mechanism of dielectric relaxation in $Y_{2/3}Cu_3Ti_{4-x}Fe_xO_{12}$ ceramic could be interpreted reasonably by the modified mixed valent structure in transition metallic oxide ceramic. In a mixed valent structure, the dielectric relaxation is supposed due to loss of traces of oxygen, creating thereby oxygen vacancies during sintering at high temperature in accordance with Kroger-Vink notation of defects with reaction

$$O_2 \leftrightarrow \frac{1}{2}O_2 + V_0^{\bullet\bullet} + 2e^- \quad (2)$$

where all the species are written in accordance with Kroger-Vink notation of defects [20]. Electrons released in this reaction may be captured by Cu^{2+} or Ti^{4+} to produce Cu^{+} or Ti^{3+} respectively as below:

$$2Cu^{2+} + 2e^- \rightarrow 2Cu^{+} \quad (3)$$

$$2Ti^{4+} + 2e^{-} \rightarrow 2\mathrm{Ti}^{3+}$$

(4)

The probability of formation of Ti^{3+} ($3d^1$) is negligible in comparison to Ti^{4+} ($3d^0$) as per stability criteria. On the other hand, Cu^{+} with $3d^{10}$ configuration is a stable state of Cu due to inert gas configuration. Cu^{+} ions on Cu^{2+} site will carry an effective negative charge, viz $Cu^{+}_{Cu^{2+}}$. These negative charges may form dipoles with $V_o^{\bullet\bullet}$ as $2Cu^{+}_{Cu^{2+}} \rightarrow V_o^{\bullet\bullet}$. These diploes can change their orientation either by hopping of electron among Cu^{+} and Cu^{2+} or due to jumping of oxygen ions through vacant oxygen sites around the CuO_4 square or TiO_6 octahedral giving rise to orientation polarization. It leads to increase in the conductivity and so the dielectric loss as observed in Fig 7, discussed later. Increase in conductivity makes the grain of such mixed-valent ceramics to be semiconducting. The rapid decrease in dielectric constant of $Y_{2/3}Cu_3Ti_{4-x}Fe_xO_{12}$ with different Fe^{3+} concentration at higher frequency may be due to inability of dipoles to keep stepping with the change in frequency. This is the reason for high frequency dielectric relaxation of YCTFO ceramic which gets induced by a mixed valent structure of Cu^{+}/Cu^{2+} and Ti^{3+}/Ti^{4+} while the low frequency dielectric relaxation of YCTFO ceramic may be regarded as a result of oxygen vacancies created during sintering process. The duo factor, the mixed valent structure and oxygen vacancies may be significantly contribute for the origin of the high dielectric constant of YCTFO ceramic. Along with these two factors interfacial polarization and formation of barrier layer at grain and grain boundaries interface significantly contribute to the high dielectric constant of YCTFO ceramic. Formation of barrier layers at interface can be further confirmed by impedance and modulus analysis.

Fig. 9 presents room temperature frequency dependent dielectric loss (tan δ) of $Y_{2/3}Cu_3Ti_{4-x}Fe_xO_{12}$ ceramic as a function of concentration of Fe^{3+} (where x = 0.00, 0.50, 0.10, 0.15, 0.20). The value of tan δ decreases rapidly over the entire frequency range which may be attributed to the presence of small interfacial polarization in the YCTFO ceramic. No constant variation in tan δ with frequency is observed for all compositions. Dielectric loss for all compositions show a sharp decreasing trend up to 100 Hz and then a small rising at 1 kHz for x = 0.00, 0.10 and 0.20 but after 1 kHz the dielectric losses decreases sharply, however the dielectric losses for YCTFO ceramic are higher at low frequency below 10 kHz. Further the tan δ value decreases significantly at a higher frequency form 10 kHz-5MHz which may be due of interfacial polarization originating in the YCTFO ceramic. Higher concentration of

Fe^{3+} doping may introduce more oxygen vacancies and space charges producing thereby dielectric relaxation peaks which cause more dielectric loss.

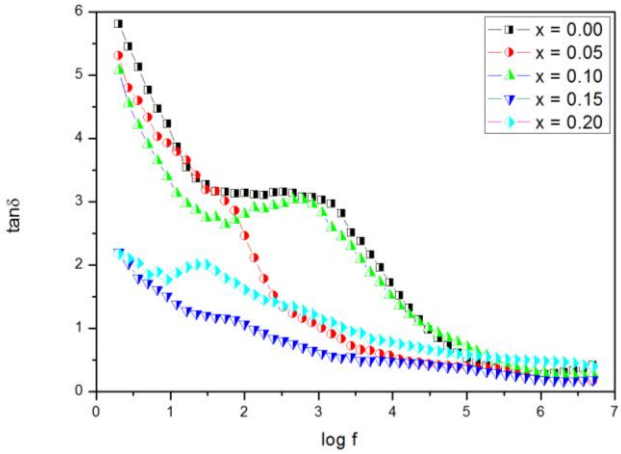

Figure 9: Plots of Loss Tangent (tan δ) with Frequency at few Selected Temperatures for $Y_{2/3}Cu_3Ti_{4-x}Fe_xO_{12}$

Ceramic (x = 0.00,0.05, 0.10, 0.15 and 0.20).

It is also clear from Fig. 9 that the curve passes through a minimum tan δ value of 2.5, 2.29, 0.94 for x = 0.00, 0.10 and 0.20 and 0.74, 0.51 for x = 0.05, 0.15 respectively at a frequency, $f = 10^{3.5}$Hz. In all, Fe^{3+} doping in YCTO ceramic can reduce the dielectric loss at high frequency ranges. The sample with x = 0.15 and 0.20 possess comparatively lower dielectric loss while sample with x = 0.00 exhibits much higher dielectric loss. For almost all compositions of YCTFO ceramics x = 0.00-0.20, the tan δ value decreases showing a clear hump at or below 10 k Hz. Further the curve for x = 0.15, 0.15 got relatively flat, with no hump, and these were similar to some extent to those of variation in dielectric constant value with increasing frequency, in contrast to a strong dependency of dielectric loss with increase in frequency for YCTFO ceramic at x = 0.00, 0.10 and 0.20 is quite surprising. The reason for such anomalous behavior of variation in dielectric loss of Fe at x = 0.00, 0.10 and 0.20 to those of x = 0.05 and 0.15 due to bimodal distribution of grain in YCTFO ceramic for different x-values, grain sizes, its distribution and grain growth phenomena of both small and larger sized grain as already discussed in microstructure section. Such anomalous trend were also reflected in variation of ε-T and tan δ-T as seen in Fig. 7 and in Fig. 8(a) supporting thereby the fact that a proportionate introduction of Fe^{3+} flattens the dielectric constant appreciably with a significant reduction in dielectric loss (tan δ) simultaneously in the YCTFO ceramic.

The decreasing value of both, ε_r and tan δ with increasing frequency are due to interfacial polarization which arises as discussed earlier, due to micro-heterogeneities arisen in the ceramic with different extent of doping. These may be present because of the slow diffusion controlled thermochemical process used in their preparation. Fe^{3+} substitution in $Y_{2/3}Cu_3Ti_4O_{12}$ (YCTO), lower downs the dielectric loss (tan δ) but the same along with give rise to higher values of ε_r as compared to the parent YCTO ceramic and it shows stronger dependence on frequency as well as temperature. This limits the usefulness of these materials. It is expected that using different atmosphere during sintering and post sintering, the above properties may be improved showing a positive direction for clues to decrease the dielectric loss to an appreciable extent for potential application of YCTFO ceramic, the next task to the researcher.

Impedance spectroscopic studies

Electrical behavior of different YCTFO samples in correlation with its microstructure could be supported by impedance analysis. A representative Cole-Cole Plots for sintered YCTFO ceramics at different concentration at room temperature is illustrated in Fig. 10. It clearly demonstrates the presence of two semi-circular arcs with different intercepts (except for x = 0.20) which may be due to the grain boundary and electrode surface effects. On extrapolation Fig. 11, the intercept on Z' axis is not found to be close to zero. It suggests that there must be an existence of another semi-circle in higher frequency region beyond the measuring frequency range. The non-zero intercepts on Z' axis give the grain resistance values which are shown in Table 5. The non-zero intercept at high frequencies is very small which indicates that the total resistance of YCTFO ceramics is governed by R_{gb} i.e. $R_{gb} >> R_g$ where R_{gb} and R_g are the resistances of grain boundary and grain, respectively and $C_{gb} >> C_g$ where C_{gb} and C_g are the capacitances of grain boundary and grain, respectively. It implies that the dielectric properties are mainly influenced by the physical characteristic of grain boundary, such as ε' i.e. the real part of permittivity, the resistivity and the thickness i.e. an exact ratio of the average grain size and the grain boundary depletion layer width. The exceptional behavior for the YCTFO ceramic with concentration variant x = 0.20 suggests the predominance of electrode effect at room temperature. Therefore IBLC effect, as well accepted for the reason of dielectric phenomena in CCTO, can be applicable to reveal the dielectric response in different YCTFO ceramics. The appeared dielectric characteristic of all the five concentration variant of YCTFO ceramics, as described under section 3.4 may be attributed to the effect of special heterogeneous microstructure [21].

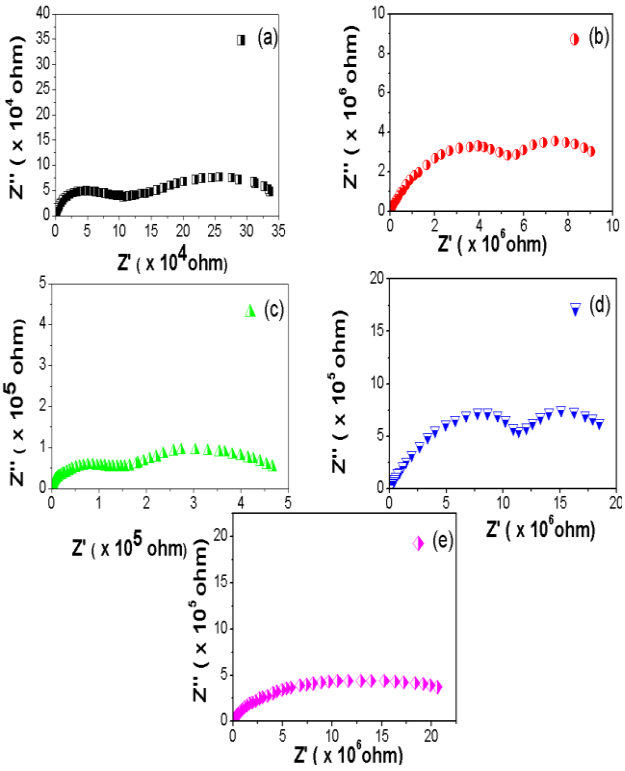

Figure 10: Complex Impedance Plane Plots (Z' vs Z'') at 308 K for Sintered $Y_{2/3}Cu_3Ti_{4-x}Fe_xO_{12}$ Ceramic (a) x =

0.00, (b) x = 0.05, (c) x = 0.10, (d) x = 0.15 and (e) x = 0.20.

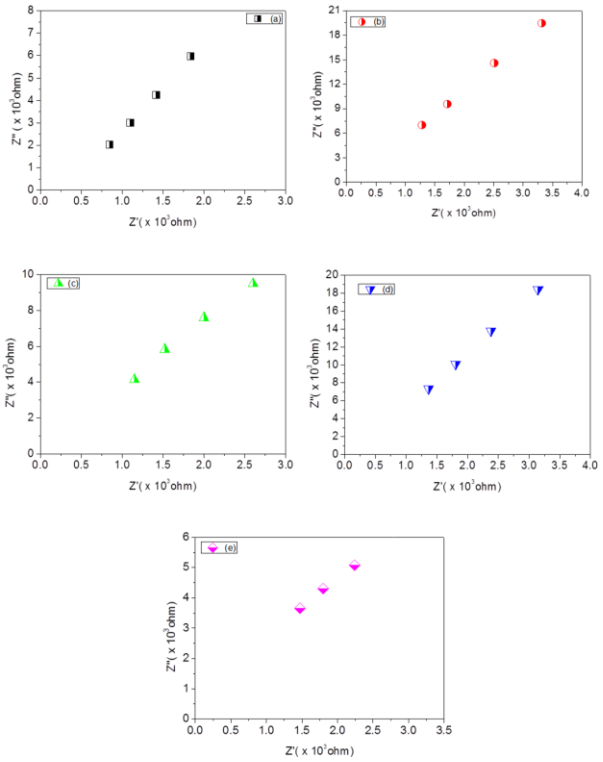

Figure 11: Extrapolation of Z′ vs Z″ plot in the High Frequency Range at 308 K to get Resistance of Grain

for$Y_{2/3}Cu_3Ti_{4-x}Fe_xO_{12}$ Ceramic (a) x = 0.00, (b) x = 0.05, (c) x = 0.10, (d) x = 0.15 and (e) x = 0.20.

Table 5: Calculated values of resistances and capacitances of grain and grain boundary at room temperature (308 K) for

$Y_{2/3}Cu_3Ti_{4-x}Fe_xO_{12}$ (x = 0.00, 0.50, 0.10, 0.15 and 0.20) nano- ceramic sintered at 1000 ^oC for 12 h.

Composition	**R_g(Ω)**	**R_{gb}(Ω)**	**C_g (pF)**	**C_{gb} (nF)**
x = 0.00	410	1.28×10^5	-	9.13
x = 0.05	379	1.21×10^5	-	9.22
x = 0.10	368	1.94×10^5	-	9.25
x = 0.15	345	1.34×10^5	-	9.29
x = 0.20	296	1.08×10^5	-	9.33

Fig. 12 discloses variation of the imaginary part of impedance Z″ with frequency at room temperature for different concentration variant of YCTFO ceramics. It displays the appearance of two relaxation peaks in two different ranges of frequencies except for x = 0.20. The relaxation peaks at lower frequency region may be due to the electrode effects whereas at high frequency region it may be due to grain boundary effects. The intensity of peaks get suppressed and slightly shifted to high frequency region on increasing temperature which also confirms the existence of a temperature-dependent Maxwell-Wagner dielectric relaxation. It is also important to note that the inflection point in the impedance plots is the same as that of relaxation peaks in the corresponding ε″ vs log f (Fig. 7b) plot. This gives a clear evidence for the occurrence of Maxwell-Wagner relaxation. A decrease in the intensity peak of different concentration variant of YCTFO ceramics also suggests a thermally activated dielectric response. The electrode resistance appears at all measured temperature which may be due to electrode polarization effects present in the YCTFO ceramic. In other words, we

can say that the dielectric property of YCTFO ceramic is due to the combined effect of grain and grain boundaries mainly.

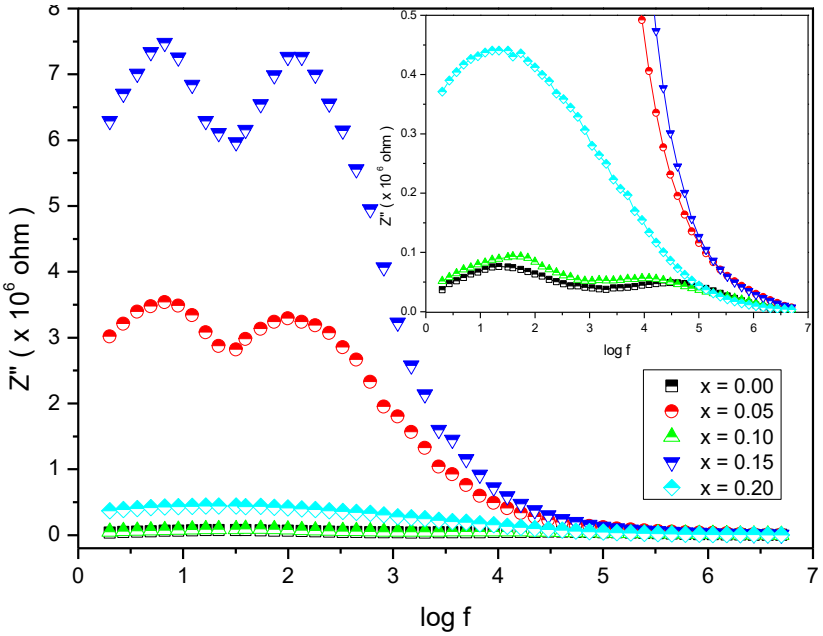

Figure 12: Variation of Z'' vs frequency at room temperature (308 K) for $Y_{2/3}Cu_3Ti_{4-x}Fe_xO_{12}$ ceramic (x = 0.00,

0.05, 0.10, 0.15 and 0.20).

CONCLUSIONS

In summary, nano-sized $Y_{2/3}Cu_3Ti_{4-x}Fe_xO_{12}$ ceramic (where x = 0.00, 0.05, 0.10, 0.15 and 0.20) was synthesized by semi-wet route using metal nitrate solution and solid TiO_2 powder in stoichiometric ratio. Single-phase formation of all the sintered ceramics was confirmed by XRD. Scanning electron micrographs shows bimodal non-uniform grain size distribution consisting of small smooth surfaced grains with some pores. Anomalous grain growth is observed in these samples. This is due to partial melting of CuO, which promotes anomalous grain growth. The dielectric property of all the five concentration variant of YCTFO ceramics is due to the combined effect of interfacial polarization and formation of barrier layer at grain and grain boundaries interface and their special heterogeneous microstructure which contribute significantly. The impedance spectroscopic analysis shows two major contributions associated with the grains and the grain boundaries.

ACKNOWLEDGEMENTS

Authors are very thankful to Prof. R K Mandal, Department of Metallurgical Engineering, IIT (BHU) for extending TEM and SEM facility.

REFERENCES

[1] A. J. Moulson, J.M. Herbert. Electroceramics, Second ed. Wiley, England, 2003.

[2] D.E. Kotecki, Integr. Ferrorlectrics **16** (1997) 1.

[3] C.C. Homes, T. Vogt, S.M. Shapiro, S. Wakimoto, A.P. Ramirez, Sci.**293** (2001) 673.

[4] M.A. Subramanian, A.W. Sleight, Solid State Sci. **4** (2002) 347.

[5] Garner CM, Kloster G, Atwood G, Mosley L, Palanduz AC. Microelectr. Reliab. **45** (2005) 919.

[6] D.C. Sinclair, T.B. Adams, F.D. Morrison, A.R. West, Appl. Phys. Lett. **80** (2002) 2153.

[7] Y. Liu, R. L. Withers, and X. Y. Wei, Phys. Rev. B **72** (2005)134104.

[8] T. B. Adams, D. C. Sinclair, A. R. West, , *J.* Am. Ceram. Soc., **89** (2006) 2833.

[9] K.D. Mandal, Alok Kumar Rai, D. Kumar, Om Parkash, J. Alloy. Comp. 478 (2009) 771.

[10] L. Jianjun, D. Chun-Gang, W. N. Mei, R. W. Smith, J. R. Hardy, J. Appl. Phys., **98** (2005) 093703.

[11] L. Pengfei, Y. Zupei, C. Xiaolian, L. Zonghua, J. Am. Ceram. Soc., **95** (2012) 2218.

[12] L. Junwei, L. Pengfei, Y. Jing, C. Xiaolian, Y. Zupei, J. Am. Ceram. Soc., **98-3** (2015) 795.

[13] Sharma Sunita, Yadav Shiv Sundar, Singh M. M., Mandal K.D, J. Adv. Dielectr., **4** (2014) 1450030-1.

[14] B. D. Culity, S.R. Stock. Elements of X-ray Diffraction, Prentice Hall, New Jersey, Chapt 1, 2001.

[15] R. Delhez, Th. H. de Kejser,; E. J.Mittemeijer, Fresenius Z. Anal. Chem. **312** (1982) 1–16.

[16] Williamson, G. K.; Hall, W. H. Acta Metall. **1** (1953) 22–31.

[17] T.T Fang., C.P. Liu. Chem Mater **17** (2005) 5167.

[18] E. Niwa, C.Uematsu, T.Hashimoto, J. Am. Ceram. Soc. **95** (2012), 3802.

[19] B. Tareev. Physics of Dielectric Materials, Mir Publication, Moscow, (1975).

[20] I. Burn, S. Neirman, J. Mater. Sci. **17** (12) (1982) 3510.

[21] E. Barsoukov, J.R.Macdonald, Second Edition, Wiley Blackwell, U.S.A. (2005).